PLOS | ONE

Iron Limitation Modulates Ocean Acidification Effects on Southern Ocean Phytoplankton Communities

Clara J. M. Hoppe[1]*, **Christel S. Hassler**[2¤], **Christopher D. Payne**[3], **Philippe D. Tortell**[3], **Björn Rost**[1], **Scarlett Trimborn**[1]

1 Alfred Wegener Institute Helmholtz Centre for Polar and Marine Research, Bremerhaven, Germany, **2** University of Technology Sydney, Plant Functional Biology and Climate Chance Cluster, New South Wales, Australia, **3** University of British Columbia, Vancouver, British Columbia, Canada

Abstract

The potential interactive effects of iron (Fe) limitation and Ocean Acidification in the Southern Ocean (SO) are largely unknown. Here we present results of a long-term incubation experiment investigating the combined effects of CO_2 and Fe availability on natural phytoplankton assemblages from the Weddell Sea, Antarctica. Active Chl *a* fluorescence measurements revealed that we successfully cultured phytoplankton under both Fe-depleted and Fe-enriched conditions. Fe treatments had significant effects on photosynthetic efficiency (F_v/F_m; 0.3 for Fe-depleted and 0.5 for Fe-enriched conditions), non-photochemical quenching (NPQ), and relative electron transport rates (rETR). pCO_2 treatments significantly affected NPQ and rETR, but had no effect on F_v/F_m. Under Fe limitation, increased pCO_2 had no influence on C fixation whereas under Fe enrichment, primary production increased with increasing pCO_2 levels. These CO_2-dependent changes in productivity under Fe-enriched conditions were accompanied by a pronounced taxonomic shift from weakly to heavily silicified diatoms (i.e. from *Pseudo-nitzschia* sp. to *Fragilariopsis* sp.). Under Fe-depleted conditions, this functional shift was absent and thinly silicified species dominated all pCO_2 treatments (*Pseudo-nitzschia* sp. and *Synedropsis* sp. for low and high pCO_2, respectively). Our results suggest that Ocean Acidification could increase primary productivity and the abundance of heavily silicified, fast sinking diatoms in Fe-enriched areas, both potentially leading to a stimulation of the biological pump. Over much of the SO, however, Fe limitation could restrict this possible CO_2 fertilization effect.

Introduction

The Southern Ocean (SO) exerts a disproportionate control on the global carbon cycle over glacial-interglacial timescales [1,2] and contributes significantly to the oceanic sequestration of anthropogenic CO_2 [3]. Besides abiotic drivers such as ocean circulation and sea-ice cover, biological carbon uptake and drawdown also control the air-sea-flux of CO_2 in the SO [1,2]. These biological processes are mediated by phytoplankton communities, dominated mainly by silicifying diatoms [4].

The surface waters of the SO are rich in major nutrients such as nitrate and phosphate, but in vast areas of this region primary production is limited by low iron (Fe) availability [5]. Both laboratory and *in-situ* fertilisation experiments have demonstrated that the growth of SO phytoplankton is strongly enhanced by the addition of Fe [6,7,8]. As Fe is a key nutrient for biochemical pathways including photosynthesis and nitrate assimilation [9], limiting Fe concentrations lead to decreased photochemical efficiencies and photosynthetic rates [10,11]. One important source of iron in open-ocean waters is the melting of sea-ice, which causes seasonal and localized phytoplankton blooms and

strong vertical particle fluxes [12,13]. These factors make the marginal sea-ice zone a biogeochemically important region of the SO [12].

The effects of seawater carbonate chemistry on SO phytoplankton have received increasing attention over recent years. Laboratory studies suggest that Antarctic phytoplankton can be growth-limited by CO_2 supply under present-day CO_2 concentrations [14,15]. Field data from continental shelf waters of the Ross Sea have demonstrated CO_2-dependent changes in primary productivity and phytoplankton assemblages [16,17]. In these prior studies, phytoplankton assemblages were not demonstrably Fe-limited (e.g. high F_v/F_m reported in [17]), making the extrapolation of results to the open SO waters difficult. Recently, pH-dependent shifts in Fe speciation have been reported [18], suggesting a strong potential for ocean acidification (OA) to reduce Fe bioavailability as seen in experiments with Arctic phytoplankton assemblages [19].

Given the Fe-limited status of much of the SO, there is a great need to investigate combined effects of OA and Fe limitation in this region. Here we present results from a CO_2-Fe-incubation experiment (190, 390 and 800 µatm pCO_2 under Fe-enriched and

Fe-depleted conditions) using an open ocean phytoplankton assemblage from the Weddell Sea, an important region for SO primary productivity. The aim of this study was to investigate the interactive effects of OA and Fe availability on species composition, primary production, as well as iron uptake and photophysiology of Fe-limited phytoplankton assemblages.

Materials and Methods

Experimental Setup

A ship-board incubation experiment was designed using a CO_2-Fe-matrix-approach to examine potential interactive effects between CO_2 and Fe availability on SO phytoplankton communities. A natural phytoplankton assemblage from the Weddell Sea (66°50′S, 0°W) was sampled during mid Dec. 2010 on the *RV Polarstern* ANT-XXVII/2 cruise. The permission for field work according to the Antarctic Treaty was issued by the Umweltbundesamt (Germany). Seawater was collected from 30 m depth using a "torpedo fish" towed outside the ship's wake [20]. To eliminate large grazers, we filtered seawater through an acid-cleaned 200 μm mesh. Water containing the natural phytoplankton community was transferred into acid-cleaned 4L polycarbonate bottles and incubated in growth chambers at $3\pm1°C$ with a constant daylight irradiance of 40 ± 5 μmol photons $m^{-2} s^{-1}$ (Master TL-D 18W daylight lamps, Philips, adjusted by neutral density screens). The applied irradiance was based on several light measurements in the SO at the sampling depth (data by Mitchell; e.g. DOI: 10.1594/PANGAEA.132802). To provide sufficient time for changes in the phytoplankton assemblages to occur and achieve ecologically relevant information, experiments lasted between 18 and 30 days depending on experimental treatment (18–20 days in case of Fe-enriched and 27–30 days in case of Fe-depleted treatments). In order to prevent significant changes in chemical conditions due to phytoplankton growth, incubations were diluted with 0.2 μm filtered seawater when nitrate concentrations were about 10 μmol kg^{-1}. Dilution water was obtained from the initial sampling location and filtered through acid-cleaned 0.2 μm filter cartridges (AcroPak 1500, PALL). Experiments were run with triplicate treatments of two Fe levels (Fe-enriched and Fe-depleted; see below) and 3 pCO_2 levels (190, 390 and 800 μatm).

Tubing, bubbling systems, reservoir carboys, incubation bottles and other equipment were acid-cleaned prior to the cruise using trace metal-clean techniques: After a 2-day Citranox detergent bath and subsequent rinsing steps with Milli-Q (MQ, Millipore), equipment was kept in acid (5N HCl for polyethylene and 1N HCl for polycarbonate materials) for 7 days, followed by 7 rinses with MQ. Equipment was kept triple-bagged during storage and experiments. Incubation bottles were stored under acidified conditions (addition of 500 μL 10N suprapure quarz destilled HCl, Carl Roth, in 500 mL MQ) and rinsed twice with seawater prior to the start of the experiment.

In order to mimic different pCO_2 conditions, the incubation bottles were continuously sparged with air of different CO_2 partial pressures (190, 390 and 800 μatm) delivered through sterile 0.2 um air-filters (Midisart 2000, Sartorius stedim). Gas mixtures were generated using a gas flow controller (CGM 2000 MCZ Umwelttechnik), in which CO_2-free air (<1 ppmv CO_2; Dominick Hunter) was mixed with pure CO_2 (Air Liquide Deutschland). The CO_2 concentration in the mixed gas was regularly monitored with a non-dispersive infrared analyzer system (LI6252, LI-COR Biosciences) calibrated with CO_2-free air and purchased gas mixtures of 150 ± 10 and 1000 ± 20 ppmv CO_2 (Air Liquide Deutschland).

To promote phytoplankton growth, 1 nM Fe ($FeCl_3$, ICP-MS standard, TraceCERT, Fluka) was added to the Fe-enriched treatments. In the Fe-depleted treatments, 10 nM of the hydroxamate siderophore desferrioxamine B (DFB, Sigma) was added to bind and thereby reduce the bioavailable Fe [21,22]. No additional macronutrients were added to the incubation bottles. Abiotic control bottles, used to assess changes in Fe chemistry, contained filtered seawater (0.2 μm) exposed to each treatment condition over the duration of the experiment.

Chemical parameters

Nutrients were determined colorimetrically on-board with a Technicon TRAACS 800 Auto-analyzer on a daily basis over the course of the experiments, following procedures improved after [23]. Samples for total alkalinity (TA) were 0.6 μm-filtered (glass fibre filters, GF/F, Whatman), fixed with 0.03% $HgCl_2$ and stored in 150 mL borosilicate bottles at 4°C. TA was estimated at the Alfred Wegener Institute (Germany) from duplicate potentiometric titration [24] using a TitroLine alpha plus (Schott Instruments). The calculated TA values were corrected for systematic errors based on measurements of certified reference materials (CRMs provided by Prof. A. Dickson, Scripps, USA; batch #111; reproducibility ±5 μmol kg^{-1}). Dissolved inorganic carbon (DIC) samples were filtered through 0.2 μm cellulose-acetate filters (Sartorius stedim), fixed with 0.03% $HgCl_2$ and stored in 5 mL gas-tight borosilicate bottles at 4°C. Also in the home laboratory, DIC was measured colourimetrically in triplicate with a QuAAtro autoanalyzer (Seal) [25]. The analyser was calibrated with $NaHCO_3$ solutions (with a salinity of 35, achieved by addition of NaCl) with concentrations ranging from 1800 to 2300 μmol DIC kg^{-1}. CRMs were used for corrections of errors in instrument performance (e.g. baseline drift). Seawater pH was measured potentiometrically on the NBS scale (pH_{NBS}; overall uncertainty 0.02 units) with a two-point calibrated glass reference electrode (IOline, Schott Instruments). Values for pH were reported on the pH_{total} scale for better comparability with other datasets. Following suggestions by Hoppe et al. [26], seawater carbonate chemistry (including pCO_2) was calculated based on TA and pH using CO_2SYS [27]. The dissociation constants of carbonic acid of Mehrbach et al. (refit by Dickson and Millero) were used for calculations [28,29]. Dissociation constants for HSO_4 were taken from Dickson [30]. Iron chemistry was analyzed using the competitive ligand exchange adsorptive cathodic stripping voltammetry using the ligand 2-(2-thiazolylazo)-p-cresol (TAC, 10 μmol kg^{-1} [31]). Total dissolved (<0.2 um) Fe concentrations were analyzed following a 45 min UV-photo-oxidation step (acid washed quartz tubes closed with Teflon lids) and concentrations were determined in triplicate using standard additions of a freshly made $FeCl_3$ standard (ICP-MS standard, TraceCERT, Fluka, 1–4 nM).

Biological Parameters

To determine the taxonomic compositions at the end of the experiment, duplicate aliquots of 200 mL unfiltered seawater were preserved with both hexamine-buffered formalin solution (2% final concentration) and Lugols (1% final concentration). Preserved samples were stored at 4°C in the dark until further analysis by inverted light microscopy (Axiovert 200, Zeiss). Additionally, species dominating the final communities were identified using scanning electron microscopy (Philips XL30) according to taxonomic literature [32]. Average biovolume of the dominant species was calculated based on representative cell size measurements [33]. Values were in good agreement with the MAREDAT database [34]. For analysis of particulate organic carbon (POC),

cells were collected onto precombusted GF/F-filters (15 h, 500°C), which were subsequently stored at −20°C and dried for >12 h at 60°C prior to sample analysis. Analysis was performed using an Automated Nitrogen Carbon Analyser mass spectrometer system (ANCA-SL 20-20, SerCon Ltd.). Samples for determination of chlorophyll a (Chl a) concentration were filtered onto 0.45 μm cellulose acetate filters (Sartorius stedim) and stored at −20°C until analysis onboard. Chl a was subsequently extracted in 10 mL 90% acetone (overnight in darkness, at 4°C) and concentrations determined on a fluorometer (10-000 R, Turner Designs), using an acidification step to determine phaeopigments [35].

Physiological assays

Primary production of the final phytoplankton assemblages was determined in 100 mL incubations after addition of a 10 μCi (0.37 MBq) spike of $NaH^{14}CO_3$ (PerkinElmer, 53.1 mCi m-mol^{-1}). From the incubations, 0.5 mL aliquots were immediately removed and mixed with 10 mL of scintillation cocktail (Ultima Gold AB, PerkinElmer) to determine the total amount of added $NaH^{14}CO_3$. For blank determination, samples were filtered and acidified immediately after ^{14}C spikes. After 24 h of incubation under acclimation light intensity, samples were filtered onto GF/F-filters, acidified with 6N HCl and left to degas overnight. Filters were then transferred into scintillation vials, to which 10 mL of scintillation cocktail was added. After ≥2 h, the samples were measured on a ship-board liquid scintillation counter (Tri-Carb 2900TR, PerkinElmer), using automatic quench correction and a maximum counting time of 5 minutes.

Maximum Fe uptake capacity of the final phytoplankton assemblages was estimated after 2–4 h dark-acclimation in 500 mL acid-cleaned PC-bottles. In case of the Fe- treatments, cells were gently concentrated by filtration over an HCl-cleaned 2 μm membrane filter (Isopore, Millipore), rinsed and resuspended in 500 mL filtered seawater from the initial sampling location in order to dispose all DFB. From this, 50 mL were taken for Chl a measurements. Subsequently, 1 nM of ^{55}Fe (Perkin Elmer, 33.84 mCi mg^{-1} as $FeCl_3$ in 0.5 N HCl) was added to each sample (both Fe- and -enriched). Generally, 2 mL were taken from all samples to determine the initial amount of ^{55}Fe. Subsequently, cells were exposed for at least 24 h to the acclimation light intensity. At the end of the incubation time, the sample was filtered onto GF/F-filters and rinsed 5 times with oxalate solution (gravity filtered, 2 min between rinses) and 3 times with natural seawater [36]. Each filter was then collected in a scintillation vial, amended with 10 mL scintillation cocktail (Ultima Gold A, PerkinElmer) and mixed thoroughly (Vortex). ^{55}Fe counts per minute were estimated for each sample on the ship-board liquid scintillation counter (Tri-Carb 2900TR, PerkinElmer), and converted into disintegrations per minute considering the radioactive decay and custom quench curves. ^{55}Fe uptake was then calculated taking into account the initial ^{55}Fe concentration and the total dissolved Fe concentration (background and added). Fe uptake rates were normalized to POC using Chl a:POC ratios from the respective treatments.

Photophysiological parameters were measured using a Fluorescence Induction Relaxation System (FIRe; Satlantic, Canada; 37). Samples were 1 h dark-acclimated prior to measurements to ensure that all photosystem II (PSII) reaction centers were fully oxidized and non-photochemical quenching (NPQ) was relaxed. The duration of the dark acclimation was chosen after testing different time intervals (data not shown). Samples were then exposed to a strong short pulse (Single Turnover Flash, STF), which was applied in order to cumulatively saturate PSII. Afterwards, a long saturating pulse (Multiple Turnover Flash,

MTF) was applied in order to fully reduce the PSII and the plastoquinone (PQ) pool. The minimum (F_0) of the STF phase and maximum (F_m) fluorescence of the MTF was used to calculate the apparent maximum quantum yield of photochemistry in PSII (F_v/F_m) according to the equation $(F_m−F_0)/F_m$. This parameter was calculated for all bottles on a regular basis (every 6–7 days). Values of these parameters as well as of the functional absorption cross section of PSII (σ_{PSII} [Å^2 quanta^{-1}]) were derived using the FIRePro software provided by Satlantic [37]. Additional fluorescence measurements were performed under increasing irradiances (21, 41, 66, 88, 110 and 220 μmol photons m^{-2} s^{-1}) provided by an external actinic light source (warm white 350 mA LEDs, ILL3A003, CML Innovative Technologies). After 5 minutes acclimation to the respective light level, the light-acclimated minimum (F_q') and maximum (F_m') fluorescence were estimated. The effective quantum yield of photochemistry in open reaction centers of PSII was derived according to the equation $(F_m'−F_q')/F_m'$ [38]. Relative electron transport rates (rETR) were then calculated as the product of effective quantum yield and applied growth irradiance of 40 μmol photons m^{-2} s^{-1}. Using the Stern-Volmer equation [39], NPQ of Chl a fluorescence under growth irradiance was calculated as $F_m/F_q'−1$. NPQ was relaxed (values <0.1) at lowest light levels for all treatments (data not shown). All measurements were conducted at the growth temperature.

Statistics

All data is given as the mean of the replicates ($n = 3$) with 1 standard deviation. To test for significant differences between the treatments, Two Way Analyses of Variance (ANOVA) with additional normality tests (Shapiro-Wilk; passed for all data shown) were performed. The significance level was set to 0.05. Statistical analyses were performed with the program SigmaPlot (SysStat Software Inc).

Results

Seawater chemistry

The initial carbonate system (pH: 7.93±0.01; DIC 2210±17 μmol kg^{-1}; TA: 2303±14 μmol kg^{-1}) shifted to experimental treatment levels (average pH of 8.39±0.02, 8.13±0.02, and 7.80±0.03 for the three CO_2 treatments) within the first 2 days of the experiment (Figure 1 A). The semi-continuous dilute-batch approach led to stable seawater carbonate chemistry over the course of the experiment (Figure 1 A). Compared to abiotic controls, drift was <8% and <5% for TA and DIC, respectively (Table 1). Initial seawater nutrient concentrations were 29 μmol kg^{-1} nitrate, 76 μmol kg^{-1} silicate and 2 μmol kg^{-1} phosphate. Over the course of the experiment, concentrations of nitrate never fell below 7 μmol kg^{-1}, while silicate and phosphate concentrations were always above 40 and 0.8 μmol kg^{-1}, respectively. Initial Fe concentration in the water sampled for incubations was 1.12±0.15 nmol kg^{-1}. In 0.2 μm filtered seawater (i.e. abiotic control treatments) enriched with 10 nM DFB, dissolved Fe concentrations remained 1.16±0.08 nmol kg^{-1} until the end of the experiment (Table 1), indicating that the experimental bottles remained free of Fe contamination. Dissolved Fe concentrations decreased in Fe-enriched seawater (1 nM Fe added, Table 1).

Photophysiology

Over the course of the experiment, we observed significant Fe-dependent differences in the apparent maximum quantum yield of PSII reaction centres (F_v/F_m; Figure 1 B; p<0.001). Average values of F_v/F_m at the end of the experiment were 0.51±0.04 and
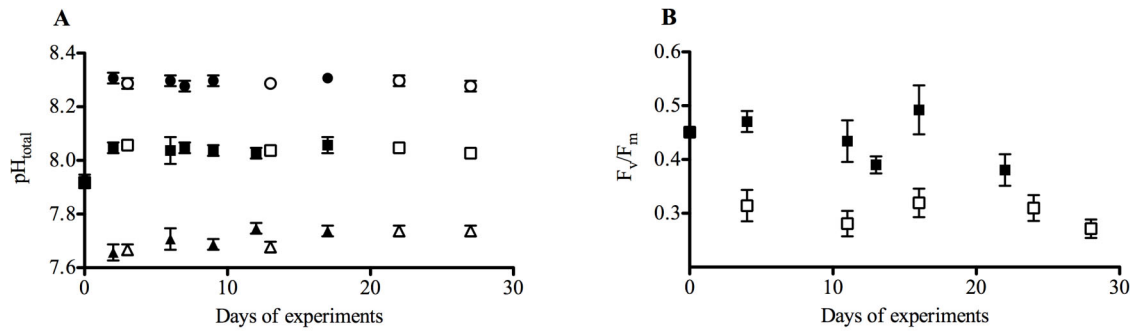
Figure 1. pH and F_v/F_m over the course of the experiment. Experimental conditions over the course of the experiment. A: Development of pH_{total} (n = 3; mean ±1 s.d.) in Fe-enriched (solid circles, 190 µatm CO_2; solid squares, 390 µatm CO_2; solid triangles, 800 µatm CO_2) and Fe-depleted treatments (open circles, 190 µatm CO_2; open squares, 390 µatm CO_2; open triangles, 800 µatm CO_2). B: Development of dark-adapted F_v/F_m (n = 3; mean ±1 s.d.) in Fe-enriched (solid squares) and Fe-depleted treatments (open squares).
doi:10.1371/journal.pone.0079890.g001

0.32 ± 0.03 for Fe-enriched and -depleted treatments, respectively (Table 2). In contrast, the pCO_2 treatments had no effects on F_v/F_m under either of the Fe treatments. Relative electron transfer rates from PSII (rETR) were significantly higher in Fe-enriched treatments, and also showed pCO_2-dependent increases under both Fe-enriched (5.7 ± 0.8 at low and 7.5 ± 0.9 at high pCO_2; p<0.001) and Fe-depleted conditions (4.2 ± 0.4 at low and 5.3 ± 0.1 at high pCO_2; p<0.001). Significant interactive effects between Fe- and pCO_2-treatments were also observed in photoprotective non-photochemical quenching (NPQ; Table 2; p<0.001). Under Fe-limitation, NPQ decreased from 0.22 ± 0.03 at low pCO_2 to 0.11 ± 0.00 at high pCO_2, while under Fe-enriched conditions, NPQ was independent of pCO_2 (0.06 ± 0.01 at all pCO_2 levels; p<0.001).

The ratios of Chl a to POC of the final phytoplankton assemblages (Table 1) were significantly higher (p<0.001) in Fe-enriched (0.023 ± 0.003 at low and 0.017 ± 0.004 at high pCO_2) compared to Fe-depleted treatments (0.012 ± 0.001 at low and 0.010 ± 0.001 at high pCO_2). Chl a:POC ratios furthermore decreased significantly with increasing pCO_2 levels (p = 0.012), irrespective of the Fe-status.

Fe and C uptake

For all pCO_2 levels, carbon-normalized Fe uptake capacities at the end of the experiment were 10-fold higher in Fe-depleted compared to Fe-enriched treatments (Figure 2; p<0.001), but with no significant CO_2 effect. Combining data across pCO_2 treatments, mean Fe uptake capacities were 7.50 ± 3.35 pmol Fe (µmol POC)$^{-1}$ h^{-1} and 0.72 ± 0.38 pmol Fe (µmol POC)$^{-1}$ h^{-1} at low and high Fe, respectively. Under Fe-enriched conditions, we observed a significant CO_2-dependent increase in C-specific primary productivity (Figure 3; p<0.001). Primary productivity increased from 4.21 ± 0.44 nmol C (µmol POC)$^{-1}$ h^{-1} at low pCO_2 to 8.15 ± 0.75 nmol C (µmol POC)$^{-1}$ h^{-1} at high pCO_2. In contrast, no CO_2-dependent productivity responses were observed in Fe-depleted treatments, with values of 3.62 ± 0.38 nmol C (µmol POC)$^{-1}$ h^{-1} at low pCO_2 and 3.93 ± 0.16 nmol C (µmol POC)$^{-1}$ h^{-1} at high pCO_2. Thus, there was a significant interactive effect of the CO_2- and Fe-treatments on NPP (p = 0.023).

Species composition

We observed pronounced shifts in the diatom-dominated phytoplankton assemblages in association with the CO_2-dependent changes in primary productivity (Figure 4; Table 3). Shifts in species composition did not lead to changes in average cell size in the different assemblages (data not shown). After Fe-enrichment, *Pseudo-nitzschia* cf. *turgiduloides* was the most abundant species under low and intermediate pCO_2 ($39 \pm 5\%$ and $40 \pm 9\%$, respectively), whereas *Fragilariopsis cylindrus* dominated communities under high pCO_2 levels ($72 \pm 5\%$). Furthermore, *Chaetoceros* cf. *simplex* abun-

Table 1. Seawater chemistry.

Treatment		Fe_{diss} [µmol kg^{-1}]		DIC [µmol kg^{-1}]		TA [µmol kg^{-1}]		pH [total]		pCO_2 [µatm]	
Initial seawater	1.12	±0.15		2071		2271		7.93		518	
+Fe	190 µatm CO_2	0.45	±0.07	2002	±11	2208	±36	8.31	±0.01	188	±6
	390 µatm CO_2	0.32	±0.04	2082	±4	2230	±8	8.06	±0.03	369	±30
	800 µatm CO_2	0.21	±0.03	2175	±14	2215	±8	7.74	±0.02	801	±51
−Fe	190 µatm CO_2	1.13	±0.16	2018	±18	2209	±5	8.28	±0.01	204	±5
	390 µatm CO_2	1.25	±0.21	2096	±41	2219	±21	8.03	±0.02	398	±22
	800 µatm CO_2	1.11	±0.09	2155	±41	2241	±52	7.74	±0.01	813	±11

Parameters of the seawater carbonate chemistry were sampled at the beginning (n = 1) and the end of the experiment (n = 3; mean ±1 s.d.). Total dissolved Fe measurements in abiotic control treatments after 0.2 µm filtration as measured by voltammetry (n = 2; mean ± 1 s.d.). The decreased dissolved Fe concentration in the +Fe treatment can be attributed to precipitation/absorption of colloidal iron. pCO_2 was calculated from TA and pH_{total} at 3°C and a salinity of 34 using CO2SYS [27], using average final nutrient concentrations of 1 and 60 µmol kg^{-1} for phosphate and silicate, respectively.
doi:10.1371/journal.pone.0079890.t001

Table 2. Physiological differences between treatments.

Treatment	Chl a: POC			F_v/F_m			σ_{PSII}			NPQ			rETR		
+Fe 190 µatm CO2	**0.023**	**±0.003**	**F[Fe]=59.57**	**0.55**	**±0.02**	**F[Fe]=162.69**	**270**	**±37.1**	**F[Fe]=36.89**	**0.06**	**±0.00**	**F[Fe]=166.34**	**5.72**	**±0.78**	**F[Fe]=59.03**
390 µatm CO2	0.025	±0.005	**p[Fe]<0.001**	0.50	±0.03	**p[Fe]<0.001**	230	±34.9	**p[Fe]<0.001**	0.05	±0.02	**p[Fe]<0.001**	5.47	±1.32	**p[Fe]<0.001**
800 µatm CO2	0.017	±0.004	F_CO2=6.84	0.52	±0.01	F_CO2=0.02	229	±19.5	F_CO2=5.29	0.06	±0.01	F_CO2=0.34	7.5	±0.87	F_CO2=22.75
−Fe 190 µatm CO2	0.012	±0.001	**pco2=0.012**	0.31	±0.02	pco2=0.894	345	±21.1	pco2=0.136	0.22	±0.03	pco2=0.568	4.16	±0.40	**pco2<0.001**
390 µatm CO2	0.013	±0.001		0.33	±0.03		330	±26.1		0.19	±0.02	F[Fe],CO2=36.07	4.48	±0.34	
800 µatm CO2	0.01	±0.001		0.32	±0.02		301	±35.9		0.11	±0.00	**p[Fe],co2<0.001**	5.29	±0.08	

Final Chl a: POC ratios (µg:µg) and photophysiological parameters (apparent maximum quantum yield of PSII F_v/F_m, proportion of non-photochemical quenching, NPQ, functional absorption cross section of PSII (σ_{PSII} [Å^2 quanta^{-1}]), and relative electron transport rates from PSII, rETR) of the final communities grown under different CO2 and Fe levels (n=3; mean ±1 s.d.). Fe-depleted (−Fe) and Fe-enriched (+Fe) conditions were achieved by the addition of 10 nmol kg^{-1} DFB and 1 nmol kg^{-1} FeCl3, respectively. Bold p values indicate statistically significant differences between treatments (p<0.05; 2-way ANOVA).
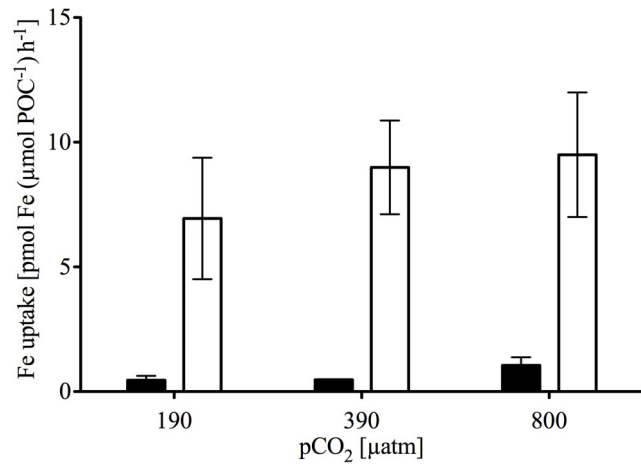doi:10.1371/journal.pone.0079890.t002

Figure 2. Iron uptake capacities of final phytoplankton communities. Fe uptake capacities [pmol Fe (µmol POC)$^{-1}$ h^{-1}] of Fe-enriched (solid bars) and -depleted (open bars) final phytoplankton communities (n=3; mean ±1 s.d.) estimated from 24 h incubation with 1 nM ^{55}Fe as a function of pCO2 [µatm]. Statistical analysis (2-way ANOVA) revealed significant differences between Fe-treatments (F=62.217, p=<0.001) but not between CO2-treatments (F=1.205, p=0.349).
doi:10.1371/journal.pone.0079890.g002

dances increased with rising CO$_2$ (from 11±0% at low pCO$_2$ to 17±1% at high pCO$_2$). Phytoplankton composition changes were also observed under Fe limitation, but the nature of these species shifts differed significantly from those seen under high Fe levels (Figure 4; Table 3). Under Fe-depleted conditions, *Pseudo-nitzschia* cf. *turgiduloides* dominated the low pCO$_2$ treatment (55±16%), while *Synedropsis* sp. was the most prevalent species under high pCO$_2$ (78±2%).
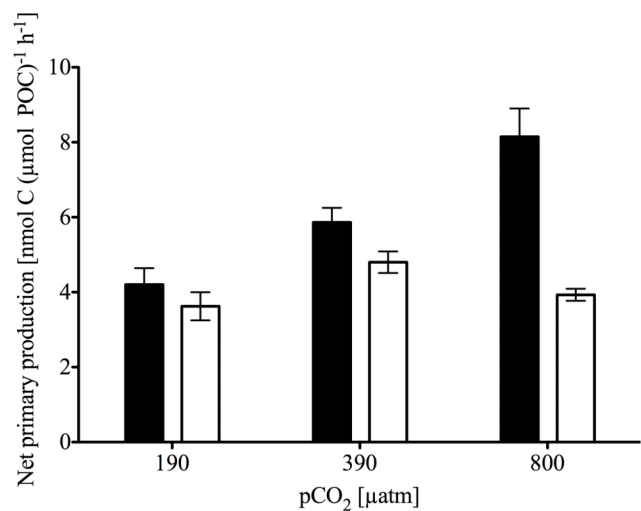

Figure 3. Net primary production of final phytoplankton communities. NPP [nmol C (µmol POC)$^{-1}$ h^{-1}] was estimated from ^{14}C incubations over 24 h as a function of pCO2 [µatm]. Black and grey bars indicate Fe-enriched (solid bars) and -depleted treatments (open bars), respectively (n=3; mean ± s.d.). ANOVA analysis revealed significant effects of pCO2 levels as well as a significant interaction term of [Fe] and pCO2 levels (F[Fe]=0.01, p[Fe]=0.92; F_pCO2=15.56, p_pCO2<0.001; F[Fe],pCO2=5.85, p[Fe],pCO2=0.023).
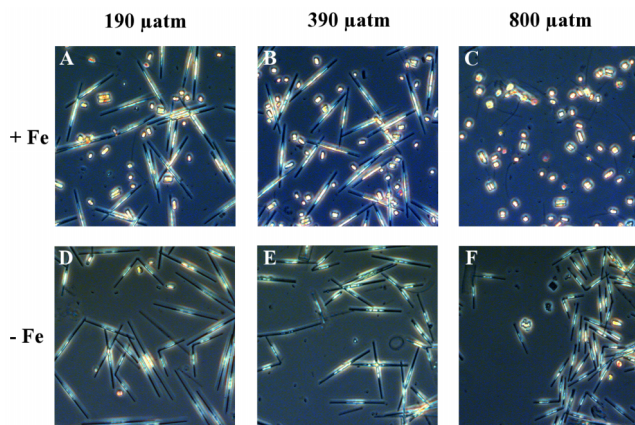doi:10.1371/journal.pone.0079890.g003

Figure 4. Representative microscopy pictures of species composition of the final communities. A, Fe-enriched 190 µatm (39±5% *Pseudo-nitzschia*, 43±4% *Fragilariopsis*); B, Fe-enriched 390 µatm (40±9% *Pseudo-nitzschia*, 42±12% *Fragilariopsis*); C, Fe-enriched 800 µatm (72±5% *Fragilariopsis*); D, Fe-depleted 190 µatm (55±16% *Pseudo-nitzschia*, 26±20% *Synedropsis*); E, Fe-depleted 390 µatm (51±15% *Pseudo-nitzschia*, 29±16% *Synedropsis*); F, Fe-depleted 800 µatm (78±2% *Synedropsis*).
doi:10.1371/journal.pone.0079890.g004

Discussion

Confirmation of Fe limitation

Dissolved Fe concentrations in Fe-depleted abiotic controls remained at initial concentrations, showing that experimental manipulations and CO_2 bubbling resulted in no significant Fe contamination (Table 1). In Fe-enriched abiotic controls, dissolved

Fe concentrations decreased over the course of the experiment. This can be attributed to precipitation and absorption of colloidal iron in the absence of significant concentrations of Fe-binding ligands [40]. Fe limitation of phytoplankton in the DFB treatments was confirmed by significant differences in F_v/F_m between Fe-enriched and -depleted treatments (Table 2; Figure 1 B). F_v/F_m values of Fe-depleted treatments are comparable to those observed in naturally Fe-limited phytoplankton communities [41]. In line with previous findings on SO phytoplankton, also other photo-physiological parameters like NPQ and rETR differed significantly between Fe treatments (Table 2, [42,43]). Moreover, the significantly higher Fe uptake capacity in Fe-depleted treatments likely reflects the induction of high-affinity uptake systems and/or the selection of phytoplankton communities with greater Fe affinities [21,22]. All of these observations confirm Fe limitation in the Fe-depleted treatments.

OA response under Fe-enriched conditions

The observed CO_2-dependent increase in primary productivity under Fe-enriched conditions (Figure 3) confirms that CO_2 fixation in SO phytoplankton can be limited by carbon supply under current CO_2 concentrations [14,16]. This hypothesis is further supported by the decrease in Chl *a*:POC ratios and the increase in rETRs with increasing pCO_2 (Table 2). Similarly, Ihnken et al. [44] observed ETR_{max} in Fe-sufficient *Chaetoceros muelleri* to increase with increasing CO_2. These findings suggest that the Calvin cycle, the major sink of photosynthetic energy [9], is the rate-limiting step of photosynthesis under low pCO_2 levels. NPQ was not affected under high pCO_2, Fe-enriched conditions. Under the applied irradiance of 40 µmol photons m^{-2} s^{-1}, however, NPQ values were generally very low (Table 2) suggesting that there is little requirement for dissipation of light. For one of

Table 3. Microscopic cell counts.

Taxonomic group	Initial	+Fe						−Fe					
		190 µatm		390 µatm		800 µatm		190 µatm		390 µatm		800 µatm	
Pseudo-nitzschia cf. *turgiduloides*	5	39	±5	40	±9	3	±3	55	±16	51	±15	<0.5	
Synedropsis sp.	1	1	±1	1	±0	3	±2	26	±20	29	±16	78	±2
Fragilariopsis cylindrus	32	43	±4	42	±12	72	±5	3	±2	2	±1	5	±3
Chaetoceros cf. *simplex*	6	11	±0	10	±2	17	±1	1	±1	3	±2	1	±1
Phaeocystis antarctica	18	1	±0	2	±2	2	±1	7	±2	6	±3	5	±1
unidentified flagellates	9	3	±1	2	±2	3	±3	<0.5		<0.5		3	±1
Choanoflagellates	6	<0.5		1	±1	<0.5		4	±2	6	±3	6	±0
Ceratoneis closterium	1	<0.5		<0.5		<0.5		1	±0	1	±1	1	±0
Dinoflagellates	6	<0.5		<0.5		<0.5		1	±1	<0.5		<0.5	
Pseudo-nitzschia cf. *turgidula*	2	<0.5		<0.5		<0.5		<0.5		<0.5		<0.5	
Fragilariopsis kerguelensis	7	<0.5		<0.5		<0.5		<0.5		<0.5		<0.5	
Thalassiosira sp.	3	<0.5		<0.5		<0.5		<0.5		<0.5		<0.5	
Large *Chaetoceros* sp.	2	<0.5		<0.5		<0.5		<0.5		<0.5		<0.5	
Rhizosolenia sp.	11	-		<0.5		<0.5		<0.5		<0.5		<0.5	
Thalassiothrix sp.	1	-		-		-		<0.5		-		-	
Guinardia sp.	<0.5	-		<0.5		<0.5		-		<0.5		<0.5	
Eucampia sp.	<0.5	<0.5		-		<0.5		-		<0.5		-	
Ciliates	<0.5	-		-		-		<0.5		<0.5		<0.5	
Silicoflagellates	<0.5	-		-		-		-		<0.5		-	

Species composition of the initial community (n = 1) and at the end of the experiment (% of total cell count; n = 3; average ±1s.d.).
doi:10.1371/journal.pone.0079890.t003

the dominant species in the Fe-enriched treatments, *Fragilariopsis cylindrus*, a significant induction of NPQ was only found at irradiances larger than 200 μmol photons $m^{-2} s^{-1}$ [43]. We can therefore conclude that even when photosynthesis was carbon limited under low pCO_2, the applied irradiance was too low to induce NPQ under Fe-enriched conditions and other pathways were operated as electron sinks (e.g. midstream-oxidases [9]).

The changes in physiological responses in Fe-enriched phytoplankton assemblages were accompanied by a pronounced shift in the species composition (Figure 4; Table 3) from *Pseudo-nitzschia* cf. *turgiduloides* under low and intermediate pCO_2 to *Fragilariopsis cylindrus* under high pCO_2 levels. Likely mechanisms for this floristic shift include species-specific differences in carbon acquisition [15,45], as well as pH-mediated differences in cellular physiology, e.g. changes in electrochemical membrane potentials and ion transport processes [46]. *Pseudo-nitzschia* has also been observed to dominate in bloom situations after Fe fertilization [7], where pH increases due to biomass build-up and drawdown of CO_2. This is in line with results from CO_2 manipulations on SO phytoplankton assemblages, which were dominated by *Pseudo-nitzschia* at high pH [16]. In a laboratory study under Fe-enriched conditions, growth and rETRs of *Pseudo-nitzschia subcurvata* were unaffected by pCO_2, suggesting that this species shows little to no responses to CO_2 fertilization [15]. Our field experiment suggests that *Fragilariopsis cylindrus*, in contrast, benefited from increased pCO_2. Even though information of OA responses for this species is lacking, the related *Fragilariopsis kerguelensis* showed enhanced rETRs with increasing pCO_2 (S. Trimborn, unpublished data). We thus speculate that *F. cylindrus* increased its photosynthetic activity under elevated pCO_2, thereby outcompeting the otherwise faster growing *Pseudo-nitzschia*. Under OA, also the relative abundance of *Chaetoceros* sp. increased by 50% (Table 3), which is consistent with previous findings on SO phytoplankton assemblages [16] as well as growth responses of *Chaetoceros debilis* to increased pCO_2 [15].

OA response under Fe-limitation

The observation that under Fe-limitation, productivity was not stimulated by increasing pCO_2 (Figure 3) may indicate that Fe acts as the main limiting factor suppressing the effects of other nutrients such as inorganic carbon. Alternatively, the apparent insensitivity of primary production to OA may arise from antagonistic physiological responses to pCO_2 and pH.

Under Fe limitation, elevated pCO_2 significantly increased rETRs and decreased NPQ, while the functional absorption cross section was not affected (Table 2). These results suggest a greater electron sink associated with the Calvin cycle and thus a decreased need for energy dissipation under OA [44]. It is also known that linear electron transport (LET) towards the Calvin cycle is not the sole sink for photosynthetic energy and that, depending on the ATP demand of the cells, alternative electron pathways can play an important role (*e.g.* Mehler reaction, MOX pathway, pseudocyclic electron flow around PSI) [9]. Increased pCO_2, however, is known to decrease photorespiration and/or the need for carbon concentrating mechanism (CCMs), which would lead to a decrease in cellular ATP demand [47]. The observed increase in rETRs in Fe-limited cells at high pCO_2 levels (Table 2) may therefore rather be linked to higher LET rates than to alternative electron pathways. The higher LET, enabled by the enhanced CO_2 fixation in the Calvin cycle, could counteract the generally greater need for photoprotection under Fe limitation [42,43]. This could explain the opposing CO_2 effects on NPQ under Fe-depleted and Fe-enriched conditions. The CO_2 effect, apparent in photophysiology, is potentially masked in primary production by

co-occurring pH effects on Fe bioavailability. According to the observed decline in Fe bioavailability with decreasing pH [18,19], Fe-depleted phytoplankton would experience the greatest Fe stress under high pCO_2.

In this study, Fe-limitation was achieved by the addition of the chelator DFB. Even though DFB has been shown to form strong complexes with Fe and thereby decrease Fe availability by >90% [36], phytoplankton can still access DFB-bound Fe to some extent [48,49]. Since the phytoplankton assemblages in our DFB-treatments were strongly Fe-limited (as demonstrated by photophysiology, Fe and C uptake), bioavailability of Fe must have been largely reduced. Fe bioavailability also seems to be slightly reduced with increasing pCO_2 (Figure 2), as has been observed in natural phytoplankton communities (i.e. without any added chelators) and in studies using different chelators such as EDTA and DFB [18,19,50]. Also, Maldonado et al. [49] suggest that the in-situ organic Fe-complexes observed in the SO have similar bioavailability compared to DFB. Although the chemical nature of in-situ organic Fe-binding ligands is not fully resolved, hydroxamate siderophores have been reported [51]. It is thus possible that at least some of the organically bound Fe exhibits a similar pH-dependent bioavailability as induced by DFB, and thus may allow for the extrapolation of our results to field situations. In order to study the bioavailability of Fe associated with in-situ Fe-binding organic ligands under OA scenarios, future experiments without added chelators should be conducted. As the nature of Fe-binding ligands remains largely unknown and can vary spatially [52,53], one should address the Fe bioavailability of various compounds (e.g., humic acids, saccharids, exopolymeric substances) that were reported to affect iron biogeochemistry [36,54,55]. Furthermore, organic ligands control the bioavailability and the physico-chemistry of trace metals in general [52,56]. As some of those (Co, Cd, Zn) are also essential for phytoplankton physiology (e.g. for the activity of the carbonic anhydrase) [57], joint measurements of other trace metals as well as their ligands would be desirable.

Although primary productivity was not sensitive to OA under Fe limitation, we did observe CO_2-dependent species shifts, with *Pseudo-nitzschia* sp. dominating under low and *Synedropsis* sp. under high pCO_2 (Figure 4). The low abundances of *F. cylindrus* in Fe-depleted treatments probably reflect the rather high sensitivity of this species towards Fe limitation [43], which could be due to low Fe uptake capacities observed for this species [21]. In contrast, *Pseudo-nitzschia* has been shown to be an efficient user of Fe under limiting concentrations [58] and sporadic Fe input events [59]. Interestingly, the final proportion of *Pseudo-nitzschia* declined strongly with increasing pCO_2, irrespectively of the Fe status (Table 3), suggesting that its growth rates must have been significantly lower than those of the dominant species (*F. cylindrus* and *Synedropsis* sp. under Fe-enriched and -depleted conditions, respectively). This observation is in line with a recent study on *P. pseudodelicatissima*, whose growth rates were not affected by OA under either Fe-deplete nor -replete conditions [50]. As *Pseudo-nitzschia* generally does not seem to benefit from increased pCO_2 levels ([15,16,50], this study), one could expect OA to have a negative effect on the abundances of this genus under on-going climate change. At present, nothing is known about the Fe and CO_2 requirements of *Synedropsis* [60]. However, a possible appearance of *Synedropsis* in phytoplankton assemblages or incubation experiments might have been overlooked in past studies, as their delicately silicified frustules are very prone to dissolution [61] and not distinguishable from *Pseudo-nitzschia* by light microscopy (Figure 4).

Our results clearly demonstrate a strong difference in CO_2-dependent community structure between Fe-enriched and Fe-depleted conditions (Figure 4). To explain these shifts, more information on species-specific differences in Fe requirements, uptake, as well as allocation strategies [21,62,63], and inorganic carbon acquisition [15,16] is needed for all dominant species.

Biogeochemical implications

The findings of our study suggest that the effects of OA on primary production and community structure are strongly modulated by the prevailing Fe concentrations. Our results, and those of others [16,64], indicate a potential stimulation of the biological pump as a result of increased pCO_2 in Fe-replete regions. Under Fe enrichment and increasing pCO_2 levels, we observed a shift from weakly silicified *Pseudo-nitzschia* towards more heavily silicified *Fragilariopsis*. *Pseudo-nitzschia* remineralizes quickly in subsurface waters [65], while *Fragilariopsis* is a more efficient vector of carbon export [12]. Thus, enhanced primary production, in concert with potentially higher export efficiencies, could lead to a stronger downward flux of organic matter in Fe-replete areas under OA.

The described feedback by 'CO_2-fertilisation', however, may not operate over the broad expanse of the Fe-limited SO. These regional differences in CO_2-sensitivity might be even more pronounced in terms of carbon export efficiencies, as under Fe-depleted conditions no functional shifts in species composition were observed. Here, all assemblages were dominated by weakly silicified species such as *Pseudo-nitzschia* cf. *turgiduloides* [54] or *Synedropsis* sp. [60]. Frustules of both species are delicate and only preserved in shallow waters or under special circumstances such as large aggregation events in combination with anoxia [61,65]. Irrespective of their potential for carbon export, all species dominating our incubations are ecologically important [61,66,67]. Furthermore, both *F. cylindrus* and *P. turgiduloides* are not only characteristic sea-ice algae but also dominate phytoplankton assemblages in open waters [66,67]. In fact, most genera being characteristic for SO phytoplankton assemblages were present in initial and final phytoplankton assemblages (Table 3). Overall, species in the incubations resemble a mixture of typical open-ocean and sea-ice associated species [68–71]. Hence, our interpretations may not be restricted to sea-ice influenced habitats only.

Our results suggest that the potential 'CO_2 fertilization' effect critically depends on the availability of Fe, determining how strongly the biological pump will serve as a carbon sink in the future SO. Realistic projections of primary production and CO_2 sequestration thus remain difficult as long as scenarios for Fe input as well as its bioavailability to phytoplankton remain poorly constrained [18,72]. The results of this study furthermore highlight the need to assess combined effects of important environmental factors in order to understand and predict responses to single stressors such as OA. In this respect, irradiance levels should also be considered as a potentially interacting factor. Indeed, the level of energization has been shown to strongly influence the strength of phytoplankton responses to OA [73], suggesting that also the interaction between Fe and CO_2 availability could be modulated by light conditions. To thoroughly assess consequences of OA, multi-factorial perturbation experiments (including factors such as different Fe sources or grazing) should target physiological as well as ecological responses of SO phytoplankton assemblages.

Author Contributions

Conceived and designed the experiments: CJMH ST BR CH PDT. Performed the experiments: CJMH ST CDP. Analyzed the data: CJMH ST CH CDP. Contributed reagents/materials/analysis tools: CJMH ST BR CH PDT CDP. Wrote the paper: CJMH ST BR CH PDT. Wrote the revised manuscript: CJMH ST BR CH PDT. Wrote the response to the reviewers: CJMH ST BR CH PDT.

References

1. Moore JK, Abbott MR, Richman JG, Nelson DM (2000) The southern ocean at the Last Glacial Maximum: A strong sink for atmospheric carbon dioxide. Global Biogeochem Cycles 14: 455–475.
2. Sigman DM, Hain MP, Haug GH (2010) The polar ocean and glacial cycles in atmospheric CO_2 concentration. Nature 466: 47–55.
3. Le Quéré C, Takahashi T, Buitenhuis ET, Rödenbeck C, Sutherland SC (2010) Impact of climate change and variability on the global oceanic sink of CO_2. Global Biogeochem Cycles 24.
4. Sakshaug E, Slagstad D, Holm-Hansen O (1991) Factors controlling the development of phytoplankton blooms in the Antarctic Ocean - a mathematical model. Mar Chem 35: 259–271.
5. Martin J, Fitzwater S, Gordon R (1990) Iron Deficiency Limits Phytoplankton Growth in Antarctic Waters. Global Biogeochem Cycles 4: 5–12.
6. Timmermans KR, Gerringa LJA, de Baar HJW, van der Wagt B, Veldhuis MJW, et al. (2001) Growth rates of large and small Southern Ocean diatoms in relation to availability of iron in natural seawater. Limnol Oceanogr 46: 260–266.
7. de Baar HJW, Boyd PW, Coale KH, Landry MR, Tsuda A, et al. (2005) Synthesis of iron fertilization experiments: From the Iron Age in the Age of Enlightenment. J Geophys Res 110: C09S16.
8. Smetacek V, Klaas C, Strass VH, Assmy P, Montresor M, et al. (2012) Deep carbon export from a Southern Ocean iron-fertilized diatom bloom. Nature 487: 313–319.
9. Behrenfeld MJ, Milligan AJ (2013) Photophysiological Expressions of Iron Stress in Phytoplankton. Ann Rev Mar Sci 5: 217–247.
10. Greene RM, Geider RJ, Falkowski PG (1991) Effect of Iron Limitation on Photosynthesis in a Marine Diatom. Limnol Oceanogr 36: 1772–1782.
11. Strzepek RF, Hunter KA, Frew RD, Harrison PJ, Boyd PW (2012) Iron-light interactions differ in Southern Ocean phytoplankton. Limnol Oceanogr 57: 1182–1200.
12. Fischer G, Futterer D, Gersonde R, Honjo S, Ostermann D, Wefer G (1988) Seasonal variability of particle flux in the Weddell Sea and its relation to ice cover. Nature 335: 426–428.
13. Lizotte MP (2001) The Contributions of Sea Ice Algae to Antarctic Marine Primary Production. Am Zool 41: 57–73.
14. Riebesell U, Wolf-Gladrow DA, Smetacek V (1993) Carbon dioxide limitation of marine phytoplankton growth rates. Nature 361: 249–251.
15. Trimborn S, Brenneis T, Sweet E, Rost B (2013) Sensitivity of Antarctic phytoplankton species to ocean acidification: Growth carbon aquisition, and species interaction. Limnol Oceanogr 58: 997–1007.
16. Tortell PD, Payne CD, Li Y, Trimborn S, Rost B, et al. (2008) CO_2 sensitivity of Southern Ocean phytoplankton. Geophys Res Lett 35: L04605.
17. Feng Y, Hare CE, Rose JM, Handy SM, DiTullio GR, et al. (2010) Interactive effects of iron, irradiance and CO_2 on Ross Sea phytoplankton. Deep-Sea Res Part 1 Oceanogr Res Pap 57: 368–383.
18. Shi D, Xu Y, Hopkinson BM, Morel FMM (2010) Effect of Ocean Acidification on Iron Availability to Marine Phytoplankton. Science 327: 676–679.
19. Sugie K, Endo H, Suzuki K, Nishioka J, Kiyosawa H, Yoshimura T (2013) Synergistic effects of pCO_2 and iron availability on nutrient consumption ratio of the Bering Sea phytoplankton community. Biogeosciences 10: 6309–6321.
20. de Jong JTM, den Das J, Bathmann U, Stoll MHC, Kattner G, et al. (1998) Dissolved iron at subnanomolar levels in the Southern Ocean as determined by ship-board analysis. Anal Chim Acta 377: 113–124.
21. Hassler CS, Schoemann V (2009) Bioavailability of organically bound Fe to model phytoplankton of the Southern Ocean. Biogeosciences 6: 2281–2296.
22. Maldonado MT, Price NM (2001) Reduction and transport of organically bound iron by *Thalassiosira oceanica* (Bacillariophyceae). J Phycol 37: 298–310.

23. Grasshoff K, Kremling K, Ehrhardt M (1999) Methods of Seawater Analysis pp 600. Weinheim: Wiley-VCH.

24. Brewer PG, Bradshaw AL, Williams RT (1986) Measurement of total carbon dioxide and alkalinity in the North Atlantic ocean in 1981. In The Changing Carbon Cycle – A Global Analysis ed. JR . Trabalka, DE . Reichle, Heidelberg Berlin: Springer Verlag. 358–381 pp.

25. Stoll MHC, Bakker K, Nobbe GH, Haese RR (2001) Continous-Flow Analysis of Dissolved Inorganic Carbon Content in Seawater. Anal Chem 73: 4111–4116.

26. Hoppe CJM, Langer G, Rokitta SD, Wolf-Gladrow DA, Rost B (2012) Implications of observed inconsistencies in carbonate chemistry measurements for ocean acidification studies. Biogeosciences 9: 2401–2405.

27. Pierrot DE, Lewis E, Wallace DWR (2006) MS Exel Program Developed for CO_2 System Calculations. ed. ORNL ORNL/CDIAC-105a Carbon Dioxide Information Analysis Centre. US Department of Energy.

28. Mehrbach C, Culberson CH, Hawley JE, Pytkowicz RM (1973) Measurement of the apparent dissociation constants of carbonic acid in seawater at atmospheric pressure. Limnol Oceanogr 18: 897–907.

29. Dickson AG, Millero FJ (1987) A comparison of the equilibrium constants for the dissociation of carbonic acid in seawater media. Deep-Sea Res 34: 1733–1743.

30. Dickson AG (1990) Standard potential of the reaction: AgCl(s)+½ H_2(g) = Ag(s)+HCl(aq), and the standard acidity constant of the ion HSO_4^- in synthetic seawater from 273.15 to 318.15 K. J Chem Thermodyn 22: 113–127.

31. Croot PL, Johansson M (2000) Determination of Iron Speciation by Cathodic Stripping Voltammetry in Seawater Using the Competing Ligand 2-(2-Thiazolylazo)-p-cresol (TAC). Electroanalysis 12: 565–576.

32. Tomas CR, Hasle GR (1997) Identifying Marine Phytoplankton. Academic Press. 858 pp.

33. Hillebrand H, Dürselen CD, Kirschtel D, Pollingher U, Zohary T (1999) Biovolume calculation for pelagic and benthic microalgae. J Phycol 35: 403–424.

34. Leblanc K, Arístegui J, Armand L, Assmy P, Beker B, et al. (2012) A global diatom database – abundance, biovolume and biomass in the world ocean. Earth Sys Sci Data 4: 149–165.

35. Knap A, Michaels A, Close AH, Dickson A. (1996) Protocols for the Joint Global Ocean Flux Study (JGOFS) Core Measurements. In JGOFS Report Nr. 19, UNESCO, pp. 170

36. Hassler CS, Schoemann V, Nichols CM, Butler ECV, Boyd PW (2011) Saccharides enhance iron bioavailability to Southern Ocean phytoplankton. Proc Natl Acad Sci USA 108: 1076–8101.

37. Gorbunov M, Falkowski P (2004) Fluorescence Induction and Relaxation (FIRe) Technique and Instrumentation for Monitoring Photosynthetic Processes and Primary Production in Aquatic Ecosystems, Lawrence.

38. Genty B, Briantais J-M, Baker NR (1989) The relationship between the quantum yield of photosynthetic electron transport and quenching of chlorophyll fluorescence. BBA 990: 87–92.

39. Bilger W, Björkman O (1991) Temperature dependence of violaxanthin de-epoxidation and non-photochemical fluorescence quenching in intact leaves of *Gossypium hirsutum* L. and *Malva parviflora* L. Planta 184: 226–234.

40. Johnson KS, Gordon RM, Coale KH (1997) What controls dissolved iron concentrations in the world ocean? Mar Chem 57: 137–161.

41. Kolber ZS, Barber RT, Coale KH, Fitzwateri SE, Greene RM, et al. (1994) Iron limitation of phytoplankton photosynthesis in the equatorial Pacific Ocean. Nature 371: 145–149.

42. van Oijen T, van Leeuwe MA, Gieskes WWC, de Baar HJW (2004) Effects of iron limitation on photosynthesis and carbohydrate metabolism in the Antarctic diatom *Chaetoceros brevis* (Bacillariophyceae). Eur J Phycol 39: 161–171.

43. Alderkamp A-C, Kulk G, Buma AGJ, Visser RJW, Van Dijken GL, et al. (2012) The effect of iron limitation on the photophysiology of *Phaeocystis antarctica* (Prymnesiophyceae) and *Fragilariopsis cylindrus* (Bacillariophyceae) under dynamic irradiance. J Phycol 48: 45–59.

44. Ihnken S, Roberts S, Beardall J (2011) Differential responses of growth and photosynthesis in the marine diatom *Chaetoceros muelleri* to CO_2 and light availability. Phycologia 50: 182–193.

45. Tortell PD, Payne CD, Gueguen C, Strzepek RF, Boyd PW, Rost B (2008) Inorganic carbon uptake by Southern Ocean phytoplankton. Limnol Oceanogr 53: 1266–1278.

46. Taylor AR, Chrachri A, Wheeler G, Goddard H, Brownlee C (2001) A Voltage-Gated H+ Channel Underlying pH Homeostasis in Calcifying Coccolithophores. PLoS Biol 9.

47. Beardall J, Raven JA (2004) The potential effects of global climate change on microalgal photosynthesis, growth and ecology. Phycologia 43: 26–40.

48. Maldonado MT, Price NM (1999) Utilization of iron bound to strong organic ligands by plankton communities in the subarctic Pacific Ocean. Deep-Sea Res Part 2 Top Stud Oceanogr 46: 2447–2473.

49. Maldonado MT, Strzepek RF, Sander S, Boyd PW (2005) Acquisition of iron bound to strong organic complexes, with different Fe binding groups and photochemical reactivities, by plankton communities in Fe-limited subantarctic waters. Global Biogeochemical Cycles 19: GB4S23.

50. Sugie K, Yoshimura T (2013) Effects of pCO_2 and iron on the elemental composition and cell geometry of the marine diatom *Pseudo-nitzschia pseudodelicatissima* (Bacillariophyceae). J Phycol 49: 475–488.

51. Velasquez I, Nunn BL, Ibisanmi E, Goodlett DR, Hunter KA, et al. (2011) Detection of hydroxamate siderophores in coastal and Sub-Antarctic waters off the South Eastern Coast of New Zealand. Mar Chem 126: 97–107.

52. Hassler CS, Schoemann V, Boye M, Tagliabue A, Rozmarynowycz M, et al. (2012) Iron Bioavailability in the Southern Ocean. In Oceanography and Marine Biology: An Annual Review, ed. A. R. Gibson RN, Gordon JDM, Hughes RN, 1–64. London: CRC Press.

53. Shaked Y, Lis H (2012) Disassembling iron availability to phytoplankton. Front Microbiol 3: 123.

54. Laglera LM, van den Berg CMG (2009) Evidence for the geochemical control of iron by humic substances in seawater. Limnol Oceanogr 54: 610–619.

55. Hassler CS, Alasonati E, Mancuso Nichols CA, Slaveykova VI (2011) Exopolysaccharides produced by bacteria isolated from the pelagic Southern Ocean - Role in Fe binding, chemical reactivity, and bioavailability. Mar Chem 123: 88–98.

56. Gledhill M, Buck KN (2012) The organic complexation of iron in the marine environment: A review. Front Microbiol 3:69.

57. Morel FMM, Price NM (2003) The Biogeochemical Cycles of Trace Metals in the Oceans. Science 300: 944–947.

58. Marchetti A, Maldonado MT, Lane ES, Harrison PJ (2006) Iron Requirements of the Pennate Diatom *Pseudo-nitzschia*: Comparison of Oceanic (High-Nitrate, Low-Chlorophyll Waters) and Coastal Species. Limnol Oceanogr 51: 2092–2101.

59. Coale KH, Johnson KS, Chavez FP, Buesseler KO, Barber RT, et al. (2004) Southern Ocean Iron Enrichment Experiment: Carbon Cycling in High- and Low-Si Waters. Science 304: 408–414.

60. Hasle GR, Medlin LK, Syvertsen EE (1994) *Synedropsis* gen. nov., a genus of araphid diatoms associated with sea ice. Phycologia 33: 248–270.

61. Stickley CE, St John K, Koc N, Jordan RW, Passchier S, et al. (2009) Evidence for middle Eocene Arctic sea ice from diatoms and ice-rafted debris. Nature 460: 376–9.

62. Sarthou G, Timmermans KR, Blain S, Tréguer P (2005) Growth physiology and fate of diatoms in the ocean: a review. J Sea Res 53: 25–42.

63. Marchetti A, Schruth DM, Durkin CA, Parker MS, Kodner RB, et al. (2012) Comparative metatranscriptomics identifies molecular bases for the physiological responses of phytoplankton to varying iron availability. Proc Natl Acad Sci USA 109: 317–325.

64. Riebesell U, Schulz KG, Bellerby RGJ, Botros M, Fritsche P, et al. (2007) Enhanced biological carbon consumption in a high CO_2 ocean. Nature 450: 545–550.

65. Parsons ML, Dortch Q, Turner RE (2002) Sedimentological evidence of an increase in *Pseudo-nitzschia* (Bacillariophyceae) abundance in response to coastal eutrophication. Limnol Oceanogr 47: 551–558.

66. Almandoz GO, Ferreyra GA, Schloss IR, Dogliotti A, Rupolo V, et al. (2008) Distribution and ecology of *Pseudo-nitzschia* species (Bacillariophyceae) in surface waters of the Weddell Sea (Antarctica). Polar Biol 31: 429–442.

67. Kang S-H, Fryxell GA (1993) Phytoplankton in the Weddell Sea, Antarctica: composition, abundance and distribution in water-column assemblages of the marginal ice-edge zone during austral autumn. Mar Biol 116: 335–348.

68. Garibotti IA, Vernet MA, Smith RC, Ferrario ME (2005) Interannual variability in the distribution of the phytoplankton standing stock across the seasonal sea-ice zone west of the Antarctic Peninsula. J Plankton Res 27: 825–843.

69. Armand LK, Crosta X, Romero O, Pichon J-J (2005) The biogeography of major diatom taxa in Southern Ocean sediments: 1. Sea ice related species. Palaeogeogr Palaeoclimatol Palaeoecol 223: 93–126.

70. Crosta X, Romero O, Armand LK, Pichon J-J (2005) The biogeography of major diatom taxa in Southern Ocean sediments: 2. Open ocean related species. Palaeogeogr Palaeoclimatol Palaeoecol 223: 66–92.

71. Assmy P, Henjes J, Klaas C, Smetacek V (2007) Mechanisms determining species dominance in a phytoplankton bloom induced by the iron fertilization experiment EisenEx in the Southern Ocean. Deep-Sea Res Part 1 Oceanogr Res Pap 54: 340–362.

72. Boyd PW, Ellwood MJ (2010) The biogeochemical cycle of iron in the ocean. Nat Geosci 3: 675–682.

73. Rokitta SD, Rost B (2012) Effects of CO_2 and their modulation by light in the life-cycle stages of the coccolithophore *Emiliania huxleyi*. Limnol Oceanogr 57: 607–618.